APL Materials

Increased luminescent efficiency of perovskite light emitting diodes based on modified two-step deposition method providing gradient concentration

Cite as: APL Mater. 6, 111101 (2018); https://doi.org/10.1063/1.5047456
Submitted: 07 July 2018 . Accepted: 18 October 2018 . Published Online: 07 November 2018

Joo Sung Kim, Himchan Cho, Christoph Wolf, Hyung Joong Yun, Jung-Min Heo, and Tae-Woo Lee

Increased luminescent efficiency of perovskite light emitting diodes based on modified two-step deposition method providing gradient concentration

Joo Sung Kim,[1,2] Himchan Cho,[1,3] Christoph Wolf,[1,3] Hyung Joong Yun,[4] Jung-Min Heo,[1,2] and Tae-Woo Lee[1,2,3,5,6,a]

[1]*Department of Materials Science and Engineering, Seoul National University, 1 Gwanak-ro, Gwanak-gu, Seoul 08826, South Korea*
[2]*BK21 PLUS SNU Materials Division for Educating Creative Global Leaders, Seoul National University, 1 Gwanak-ro, Gwanak-gu, Seoul 08826, South Korea*
[3]*Research Institute of Advanced Materials, Seoul National University, 1 Gwanak-ro, Gwanak-gu, Seoul 08826, South Korea*
[4]*Advance Nano Research Group, Korea Basic Science Institute (KBSI), 169-148 Gwahak-ro, Yuseong-gu, Daejeon 34133, South Korea*
[5]*Institute of Engineering Research, Seoul National University, 1 Gwanak-ro, Gwanak-gu, Seoul 08826, South Korea*
[6]*Nano Systems Institute (NSI), Seoul National University, 1 Gwanak-ro, Gwanak-gu, Seoul 08826, South Korea*

(Received 7 July 2018; accepted 18 October 2018; published online 7 November 2018)

We increased the luminescent efficiency of perovskite light-emitting diodes (PeLEDs) by using a modified two-step deposition method combined with an interdiffusion process without additional solvent engineering or additive molecules. Methylammonium lead bromide ($MAPbBr_3$) polycrystalline films with nanosized grains and low electronic disorder were fabricated by a modified two-step deposition process. The as-fabricated $MAPbBr_3$ films showed gradient concentration characteristics as a result of a gradient distribution of the MABr. Also, the MABr-gradient concentration structure was intensified by the interdiffusion process, showing improved performance of $MAPbBr_3$ PeLEDs with maximum current efficiency CE_{max} = 0.861 cd A^{-1} and maximum luminance = 604 cd m^{-2} with very narrow electroluminescence spectral width. This is the highest CE_{max} among $MAPbBr_3$-based PeLEDs deposited by the two-step deposition method. https://doi.org/10.1063/1.5047456

Metal halide perovskites (MHPs) have received huge attention as a promising light harvester, showing rapid progress on power conversion efficiency reaching 23.3% with only a few years of research period.[1–3] Bulk 3-dimensional (3D) MHPs have various fundamental semiconducting properties including long carrier diffusion length,[4,5] sharp band edge,[6] and high charge carrier mobility[7] and are therefore promising candidates for next-generation optoelectronics. MHPs also have excellent properties as solid-state light emitters when the electron and hole pairs are physically confined in small nanograins or nanoparticles. The MHPs have high photoluminescence quantum yields (PLQYs),[8–10] excellent charge transport properties, low material cost, and possible low-temperature processing.[11,12] They have high color purity with narrow emission linewidths [full width at half maximum (FWHM) ≤ 20 nm][9,11] and tunable bandgap[13] that cover a wide color gamut, so they are promising candidates as emitters for next-generation displays.

Although the bright (>100 cd m^{-2}) room-temperature electroluminescence (EL) of perovskite light-emitting diodes (PeLEDs) was reported in 2014,[13,14] the efficiency is still far below the state-of-the-art efficiency of organic light-emitting diodes. The main reason is that the fundamental limitations

[a]Author to whom correspondence should be addressed: twlees@snu.ac.kr and taewlees@gmail.com. Tel.: +82-2-880-8021. Fax: +82-2-885-9671.

of 3D perovskites related to small exciton binding energy and long charge carrier diffusion length were not solved. Then, the first high-efficiency of PeLEDs comparable with the efficiency of phosphorescent OLEDs (maximum current efficiency CE_{max} = 42.9 cd A^{-1}) was achieved by additive-based nanocrystal pinning (NCP), fine stoichiometry control, and use of a high-work function (WF) conducting polymer anode.[15,16] PeLEDs with outstanding EL efficiency have been further achieved using various strategies such as excess ammonium ions,[17–19] mixed cations,[20–22] self-organized multiple quantum wells,[23–29] and colloidal quantum dots (QDs).[30–34] The high efficiencies higher than 10% were achieved using the multiple-quantum-well structure, precise chemical modification, and dimensionality control.[19,22,23,25,27,32,35]

The simplest method to fabricate the MHP films by the solution process is a one-step solution process, in which stoichiometric precursors, mainly lead halide and methylammonium halide (MAX), are dissolved in polar solvents and then deposited by evaporation of the solvent.[13] However, although the one-step method achieves MHPs that have great semiconducting properties, the films have poor morphology with huge pinholes and large cuboids. As a result, these films suffer from non-radiative recombination at the surface and leakage current through direct contacts between carrier transport layers and are therefore not suitable for use in optoelectronic devices.[36–38] The poor morphology has been attributed to the poor wettability and high nucleation barrier of MHPs on a conventional carrier transport layer such as PEDOT:PSS. Various strategies such as polymer additive composite,[39–41] solvent engineering,[15,42] and surface modification[22,43] improved the coverage and device performance, but methods to control crystallization kinetics are lacking, so the resulting morphology has remained inhomogeneous.

To overcome these limitations and realize high-quality MHP films with ideal semiconducting properties, a two-step deposition method has been developed.[44] It has the great advantages of controllable deposition parameters of each precursor, so crystallization kinetics can be precisely controlled to obtain perfect pinhole-free morphology with high reproducibility.[45–47] Also, the separate deposition of each precursor enabled deep understanding of the reaction principle, and this understanding has guided the development of comprehensive design schemes to achieve the desired morphology for perovskite optoelectronic devices.[48]

However, most reported two-step deposition methods have been developed to form defect-free large crystals for photovoltaic applications,[46] but these crystals are not suitable for PeLED applications, in which carriers must be confined spatially in nanograins to achieve high radiative recombination efficiency.[15] Also, currently reported PeLEDs fabricated using two-step methods have shown very low luminance efficiency ($MAPbBr_3$:CE_{max} = 0.1 cd A^{-1}, $CsPbBr_3$:CE_{max} = 7.6×10^{-2} cd A^{-1}).[49,50] Furthermore, the luminescent characteristics and electronic properties of these PeLEDs have not been precisely analyzed.

In this study, we fabricated high-quality $MAPbBr_3$ thin films with nanosized-grains and low electronic disorder by using the two-step deposition method without any additional solvent engineering or incorporation of additive molecules. We fabricated $MAPbBr_3$ films with vertical gradient concentration and efficient carrier localization in the highly luminescent MA-doped region. Detailed analysis based on the XPS depth profile and ultraviolet photoemission spectroscopy (UPS) measurement evidenced vertically gradient composition and an energy level in $MAPbBr_3$ from the two-step deposition method, indicating *in situ* formed gradient concentration from gradual infiltration of the MABr solution into the as-deposited $PbBr_2$ layer. Also, providing an interdiffusion process during the two-step deposition process resulted in a wider MA-rich region with improved luminescent efficiency, obtaining a current efficiency of 0.861 cd A^{-1}, which is the best performance among the reported 3D PeLEDs fabricated by the two-step deposition process based on $MAPbBr_3$ without any post-treatment and additives.

The PeLEDs based on polycrystalline $MAPbBr_3$ [Fig. 1(a)] are composed of indium tin oxide (ITO)/self-organized gradient buffer hole-injection layer (Buf-HIL) (50 nm)/$CH_3NH_3PbBr_3$ (~200 nm)/1,3,5-tris (2-N-phenylbenzimidazolyl) benzene (TPBi) (50 nm)/LiF (1 nm)/Al (100 nm). The ITO substrate with sheet resistance R_S ~ 10 Ω was cleaned by sonication for 15 min each in acetone and isopropyl alcohol (IPA); then, the solvent was rapidly removed by IPA boiling on a hot plate at 300 °C. The cleaned ITO substrate was subjected to UV-ozone treatment for >15 min to develop a hydrophilic surface. A Buf-HIL solution composed of PEDOT:PSS (Clevios P VP AI4083)

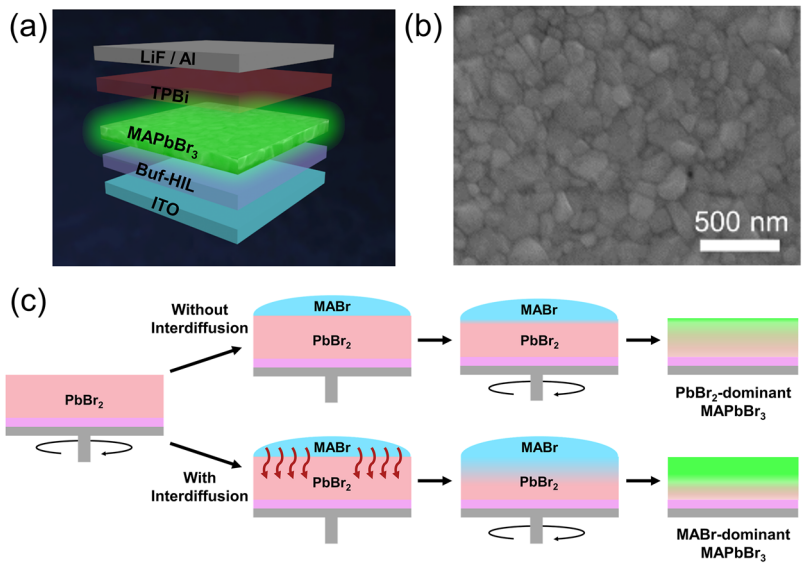

FIG. 1. (a) Schematic illustration of the device structure. (b) Top-view SEM image of the $MAPbBr_3$ polycrystalline film deposited by a modified two-step deposition process. (c) Schematic illustration of the two-step deposition method with and without the interdiffusion process.

and tetrafluoroethylene-perfluoro-3,6-dioxa-4-7-octene-sulfonic acid copolymer (PFI) (Sigma-Aldrich) in 1:1 wt. % ratio was spin-coated onto the substrate at 4500 rpm for 90 s, obtaining a 50-nm-thick Buf-HIL layer. The samples were then placed on a hot plate at 150 °C for 30 min in ambient atmosphere to form a self-assembled hole injection layer (HIL) with a gradient work function, which can facilitate hole injection into the emitting layer.

To form the $MAPbBr_3$ emitting layer, a modified two-step deposition process based on a previously reported sequential deposition method was conducted.[46] First, 1.07M of $PbBr_2$ in Dimethylsulfoxide (DMSO) solution was deposited onto the Buf-HIL layer at 8000 rpm for 15 s in a nitrogen-filled glove box and then annealed at 70 °C for 10 min to yield an ultra-smooth $PbBr_2$ thin film (Fig. S1). Then 0.16M MABr in isopropyl alcohol (IPA) solution was loaded onto the $PbBr_2$ layer and spin-coated at 3000 rpm for 90 s without acceleration time. Because MHPs obtained by conventional two-step methods have suffered from remnant $PbBr_2$, we provided an additional delay time of 15 s before spin-coating of the MABr solution on the $PbBr_2$ film. This modified process could provide sufficient penetration of the MABr solution into the underlying layer; in this paper, this is called the interdiffusion process (Fig. 1). For comparison, pristine samples deposited by the two-step method were not given any delay time. All films were then annealed at 90 °C for 10 min. The samples were then transferred to a high-vacuum thermal evaporator ($<10^{-7}$ Torr); then, TPBi (50 nm), LiF (1 nm), and Al (100 nm) were deposited at rates of 1, 0.1, and 3 Å s^{-1}, respectively. The PeLED samples were moved to a nitrogen-filled glove box and then encapsulated in N_2 atmosphere.

The quality of the resulting $MAPbBr_3$ thin films was affected by the processing method. The film produced using the modified two-step method was composed of small grains with sizes of 187 ± 79 nm and a thickness of ~200 nm with columnar structure (Fig. S2). These films showed high-quality morphology without pinholes [Fig. 1(b)]. By contrast, $MAPbBr_3$ films deposited using the conventional one-step solution process yielded micron-sized cuboid islands with poor coverage (Fig. S3), so these films suffer from leakage current and non-radiative recombination and therefore are not useful as emitters in LEDs.

The average grain size in the $MAPbBr_3$ films obtained by the two-step method was even smaller than that in the $MAPbBr_3$ films deposited by the solvent-assisted nanocrystal pinning (NCP) method (Fig. S4). This reduction in grain size can be achieved from the high concentration of the MABr solution, which can facilitate spontaneous formation of $MAPbBr_3$ with high nucleation density on top of a $PbBr_2$ film.[51] Small grain size can prevent luminescence quenching by spatial confinement

and thereby increase radiative recombination efficiency.[15] Therefore, the two-step method is a promising strategy to fabricate highly luminescent perovskite thin films with spatial confinement.

We analyzed the optical and electrical properties of $MAPbBr_3$ films obtained using different deposition methods, by using temperature-dependent UV-Vis absorption analysis. For comparison, pinhole-free $MAPbBr_3$ films deposited by a simple one-step method with the NCP method were used. In general, the electronic disorder of semiconducting materials can be depicted as[52]

$$\alpha(\mathrm{E,T}) = \alpha_0 \exp\left(-\sigma(T)\frac{E - E_g}{k_B T}\right), \tag{1}$$

where α(E, T) is the absorption coefficient as a function of energy E (eV) and temperature T (K), α_0 is a fitting parameter, σ(T) is a steepness parameter correlated with the average phonon energy, and E_g (eV) is the absorption edge energy. The Urbach energy E_U can be obtained as $E_U = k_B T/\sigma(T)$. This form demonstrates that E_U can be extracted from the inverse of the slope of the linear fit of the absorption data below the energy-gap by taking the logarithm (Fig. S5).

σ(T) can be expressed in terms of the average phonon energy ($\hbar\omega_{ph}$) by a model of Redfield and Dow[53,54] as

$$\sigma(\mathrm{T}) = \sigma_0\left(\frac{2k_B T}{\hbar\omega_{ph}}\right)\tanh\left(\frac{\hbar\omega_{ph}}{2k_b T}\right), \tag{2}$$

which is the lead-halide vibration mode of ~16 meV and which matched well with the coupling between longitudinal optical (LO)-phonons and charge-carriers.[55,56] σ(T) was obtained [Fig. 2(a)] for MHP films obtained by the single-step or two-step process. Both lines show a discontinuity of the steepness parameter at ~150 K, at which $MAPbBr_3$ changes from the tetragonal phase to the cubic phase. The films deposited using a two-step process showed slightly blue shifted phonon energy and

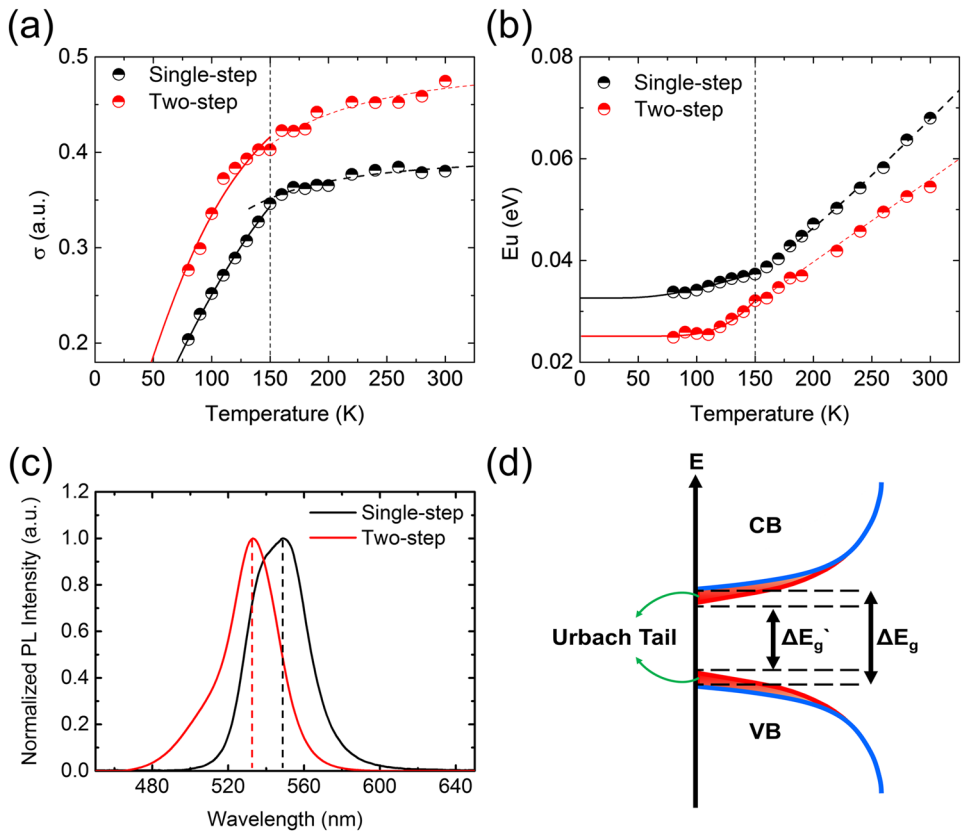

FIG. 2. (a) Steepness parameter σ vs temperature T. Solid line: fitting at $T < 150$ K; dashed line: fit at $T > 150$ K. (b) Fitted result of disorder energy E_u vs T [lines as in (a)]. (c) Normalized PL intensity of $MAPbBr_3$ films with different deposition processes. (d) Schematic representation of the Urbach tail.

rather unchanged phonon energy after the phase transition under ~150 K, which can be attributed to suppressed energy transfer via hydrogen bonding between MA and Br at low temperatures.[48] This might be a result of overall non-stoichiometric characteristics, which result in systematic change in temperature dependence in absorption characteristics[57] in MHP films deposited by the two-step process, which will be discussed below.

The temperature dependence of σ(T) was converted to electronic disorder (Urbach) energy as

$$\mathrm{E_U}(T,x) = E_1(x) + \frac{E_2}{\exp\left(\frac{\Theta}{T}\right) - 1}, \tag{3}$$

where $E_1(x)$ represents the structural disorder and $E_2(T)$ represents the thermal disorder.

The relationship of E_U to T was different in the single-step deposited films than in the two-step deposited films [Fig. 2(b)]. The data were fitted in two sections divided at ~150 K, at which the phase transition occurs; at all T, E_U was lower in the two-step deposited film than in the one-step deposited film. Considering that the NCP process during the single-step deposition method induces rapid crystallization, the lower E_U in the two-step deposition method can be attributed to slow and stable crystallization during the process without any change in supersaturation of the solution. Comparison of steady-state PL spectra [Fig. 2(c)] gives further evidence that E_U was lower after the two-step method than after the one-step method. In normalized PL spectra, the $MAPbBr_3$ film deposited by the two-step method had weaker PL intensity in the low-energy region than the $MAPbBr_3$ films deposited by the single-step method, and the PL peak was blue shifted from 533 nm in the films fabricated by the two-step method compared with the peak at 549 nm in films fabricated using the one-step method. The blue-shifted PL peak position of the film deposited using the two-step method indicates that the emission in the Urbach tail is more effectively suppressed than in the film deposited using the single-step method; this conclusion corresponds with the disordered mid-gap state [Fig. 2(d)].

In $MAPbBr_3$ films deposited by the two-step deposition method, the effect of the interdiffusion process on the luminescent property was investigated by steady-state PL measurement. Interdiffusion time of 15 s was selected as the maximum that would not cause residual MABr precipitation onto $MAPbBr_3$ films; this decision was based on comparison of X-ray Diffraction peaks and scanning electron microscopy (SEM) images (Figs. S6 and S7) with various interdiffusion times.

In $MAPbBr_3$ films without the interdiffusion process, PL emission spectra [Fig. 3(a)] measured at the top side and bottom side showed an emission peak at 533 nm that corresponds to typical polycrystalline $MAPbBr_3$ perovskites and a blue shifted additional shoulder peak at 504 nm. The PL spectra were deconvoluted (Fig. S8) with high precision ($r^2 > 0.99$) into two Gaussian peaks. According to previous reports, blue shifted emission in $MAPbI_3$ perovskites has been attributed to disordered states that mainly arise from grain boundaries.[58,59] In our case, the blue shifted shoulder peak may occur because the incomplete reaction between MABr and $PbBr_2$ yields a disordered $PbBr_2$-rich phase with a wide bandgap.[60,61] The relative intensity of the blue shifted peak was much higher at the bottom side than on the top; this difference indicates that the concentration of the $PbBr_2$-rich phase was higher on the bottom side than on the top, as a result of insufficient penetration of the MABr solution into the $PbBr_2$ film.

On the other hand, $MAPbBr_3$ samples treated using the interdiffusion process showed four times higher PL intensity at 533 nm, with negligible proportion of the shoulder peak at a higher bandgap, when measured at the top side [Fig. 3(b)]. The increased PL intensity and suppressed shoulder peak can be attributed to the increase in reaction time and penetration depth of the MABr solution into the $PbBr_2$ layer, with a consequent increase in the conversion ratio to $MAPbBr_3$ and formation of a highly luminescent MA-rich region at the top surface. However, the abnormal shoulder peak was strong in the PL spectrum measured at the bottom side, although the proportion of this peak was smaller than that in the pristine film. The results indicate that the two-step method generates hetero-structured $MAPbBr_3$ films with two regions, a highly luminescent MA-rich top side and an MA-deficient bottom side.

To further elucidate the specific structure of as-prepared $MAPbBr_3$ films, we conducted the XPS depth profile. The XPS spectra of ITO/Buf-HIL/$MAPbBr_3$ films were measured using a method reported previously.[15] In the XPS depth profile [Figs. 3(c) and 3(d)], the concentration of MA was extracted by the equivalent stoichiometric ratio between MA and carbon; this concentration was the

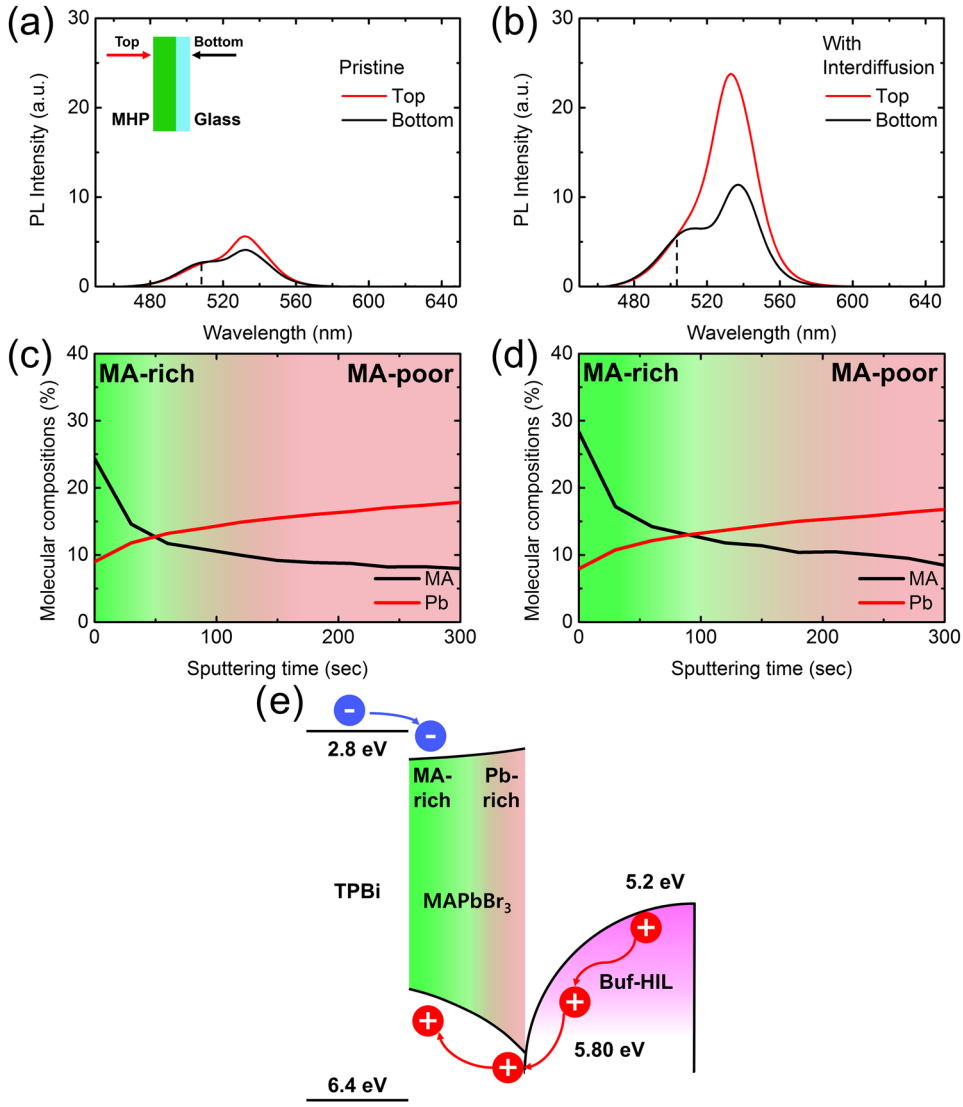

FIG. 3. Steady-state PL spectra measured at the top and bottom side of (a) pristine $MAPbBr_3$ film, (b) $MAPbBr_3$ film with the interdiffusion process. XPS depth profile of (c) pristine $MAPbBr_3$ film, (d) $MAPbBr_3$ film with the interdiffusion process, and (e) schematic diagram of the gradient doped energy level by the two-step method.

highest at the surface and gradually decreased as sputtering time increased, while the Pb composition showed the opposite trends. This gradual change in atomic concentration of the $MAPbBr_3$ film can be seen as a gradient concentration of MA; this process yields a p-doped top surface and an n-doped bottom surface. This inference is supported by a recent report that showed MAI-rich and MAI-poor regions in $MAPbI_3$ perovskites, and consequent p-doped and n-doped regions, as evidenced by the contact potential difference (CPD) between two perovskite layers that had different MAI-to-PbI_2 ratios.[62] In our case, the gradient concentration can be obtained by the gradient penetration of the MABr solution into the as-prepared $PbBr_2$ layer during the two-step method because limited MABr diffusion causes limited expansion of the $MAPbBr_3$ phase deep into the film.[51]

The effect of the interdiffusion process can be explained by the depth profile of the MA:Pb ratio. In the pristine $MAPbBr_3$ film, the MA:Pb atomic ratio at the surface was of 2.7:1, but decreased to 1:1 at a sputtering time of 60 s and further decreased with further increase in sputtering time [Fig. 3(c)]. By contrast, the $MAPbBr_3$ film treated using the interdiffusion process showed an MA:Pb atomic ratio of 3.56:1 at the surface, but decreased to 1:1 at 120 s of sputtering time [Fig. 3(d)]. The difference in

sputtering times required to reach MA:Pb = 1:1 indicates that the interdiffusion process can increase the time available for the MABr solution to penetrate into the $PbBr_2$ layer and thereby extend the MA-doped region about twice as deep as in the $MAPbBr_3$ film without the interdiffusion process. Heavily MA-doped nonstoichiometric $MAPbBr_3$ increases the luminescence efficiency,[17,63,64] so our result matches well with the dramatically increased PL intensity at the top of the $MAPbBr_3$ film that had been produced using the interdiffusion process.

Next, we conducted ultraviolet photoemission spectroscopy (UPS) measurement to verify the energy level with gradient composition distribution (Fig. S9). The work function was calculated by subtracting the secondary cutoff from the excitation radiation energy (He I, 21.2 eV), and the Fermi level energy was considered to be 0 eV. The IE that corresponds to the valence band maximum (VBM) was determined by adding the WF to the energy offset between WF and the ionization potential (IE); this offset was calculated to be 0.82 eV for both cases. When interdiffusion time was provided, IE decreased from 5.77 eV to 5.66 eV; the change can be attributed to the higher MA concentration at the surface as a result of the interdiffusion process and consequent decrease in molar proportion of insulating $PbBr_2$ at the surface. Thus, the gradient increase of MA concentration toward the top surface could result in a gradient decrease in IE. The schematic energy diagram [Fig. 3(e)] of the as-prepared $MAPbBr_3$ films by the two-step method shows this gradient energy level. As a result of the gradient in the MA:Pb ratio that was enabled by the two-step method, the MA-doped top region has higher VBM and smaller bandgap with *in situ* passivated $MAPbBr_3$ crystals with high PL efficiency, compared to the bottom region. By contrast, the MA-deficient bottom region has relatively less transporting nature and lower PL efficiency than that at the top region due to the high molar proportion of $PbBr_2$. Also, an evident shoulder peak observed at shorter wavelength can be explained by emission coming from the $PbBr_2$-rich bottom region with a larger bandgap compared with the top region. The interdiffusion process further increased the MA ratio at the surface and widened the MA-doped region at the top; as a result, radiative recombination efficiency was improved.

We fabricated PeLEDs based on $MAPbBr_3$ films produced a using two-step deposition method and measured their current-voltage-luminance characteristics. PeLEDs treated by the interdiffusion process had six times higher CE_{max} = 0.861 cd A^{-1} than those produced without the treatment with CE_{max} = 0.150 cd A^{-1} [Fig. 4(a)]. To the best of our knowledge, this is the highest ever reported CE_{max} among 3D PeLEDs based on the two-step deposition method, including $MAPbBr_3$ and pure-inorganic $CsPbBr_3$.[49,50] The interdifffusion process also increased L_{max} from 445 cd m^{-2} to 607 cd m^{-2}; this change can be attributed to the extended MA-doped region and to suppressed non-radiative recombination due to the passivation effect of the high concentration of MABr[17] [Fig. 4(b)]. Consistent with the CE_{max} tendency, the external quantum efficiency (EQE) of PeLEDs with the interdiffusion process was higher than that of pristine PeLEDs over the entire luminance intensity [Fig. S10(a)]. Furthermore, while the pristine devices showed 50% decreased EQE at a brightness of 444 cd m^{-2}, PeLEDs with the interdiffusion process showed a higher brightness of 607 cd m^{-2} at the point EQE decreased by 50% [Fig. S10(a)], which can be attributed to suppressed defect-assisted non-radiative recombination and efficient bimolecular radiative recombination at the MA-rich passivated region.[65,66] Also, to further address with the complex behavior of PeLEDs including gradual rise and roll-off of EQE (discussed in the supplementary material), we considered EQE rise and EQE roll-off with current density at each point, i.e., EQE_{max} (J_{max}) and EQE_{half} (J_{half}). We can thus define the roll-off factor

$$R = \frac{J_{half}}{J_{max}}, \tag{4}$$

which can quantify the relatively increased ratio of current density from the point at maximum quantum efficiency to that with 50% roll-off. Considering this factor, while pristine devices (R = 2.61) showed 50% roll-off up to 2.61 times higher current density compared with its J_{max}, PeLEDs with the interdiffusion process (R = 3.35) showed 50% roll-off at 3.35 times higher current density of J_{max} [Fig. S10(b)]. The result indicates slightly decreased roll-off of PeLEDs with the interdiffusion process compared to that of pristine devices. Also, this matches well with roll-off behavior considering the luminance-EQE graph, showing a similar degree of roll-off at high brightness.

The normalized EL peak showed a narrow (FWHM ~ 22 nm) single peak at 535 nm without the shoulder peak at 515 nm that was observed in PL spectra. This lack of a peak may be attributed to

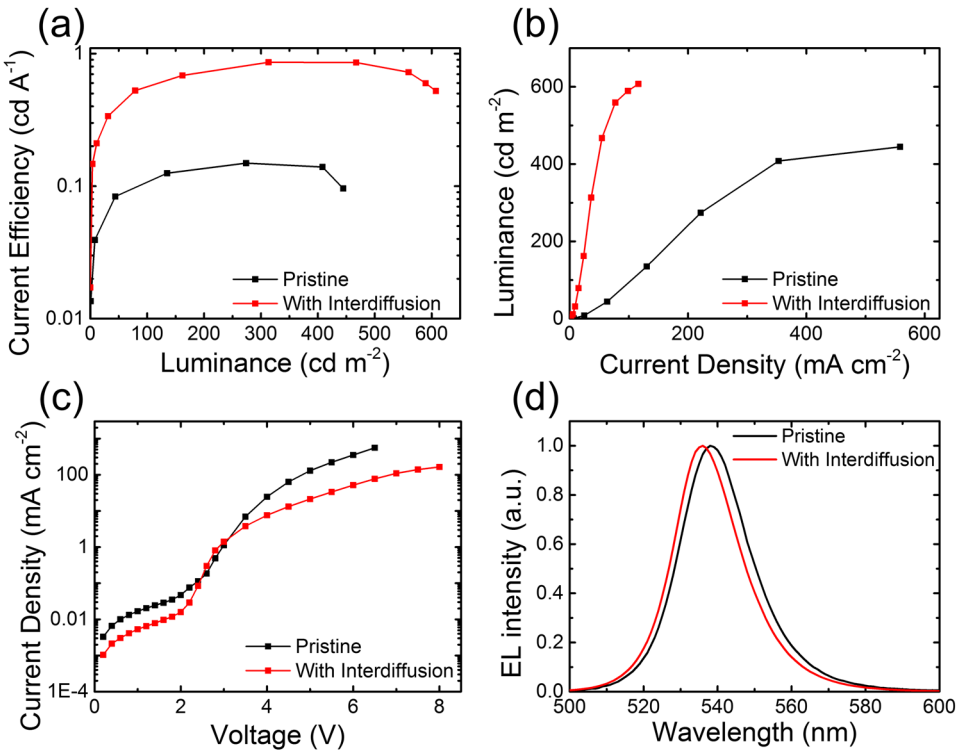

FIG. 4. (a) CE versus luminance, (b) luminance versus current density, (c) current density versus voltage, and (d) EL spectra of $MAPbBr_3$ PeLEDs deposited by the two-step method.

efficient carrier localization at the MA-doped top region from the gradient bandgap and consequent emission with narrow FWHM from pure $MAPbBr_3$. Furthermore, in PeLEDs based on films fabricated using the interdiffusion process, the EL peak was blue shifted by ~2 nm and its FWHM was narrowed slightly [Fig. 4(d)] compared with that of PeLEDs without the interdiffusion process. The blue shift of emission spectra can be attributed to passivation of shallow trap density, enabled in this case by excess MABr surrounding $MAPbBr_3$ crystals in the MA-doped top region.[67]

In conclusion, we have demonstrated a promising two-step deposition method to increase the luminescent efficiency of PeLEDs without any additive molecules or solvent engineering. As-deposited $MAPbBr_3$ films showed excellent morphology with nanosized grains and low electronic disorder energy, which are the essential characteristics for the state-of-the-art PeLEDs. Detailed analysis on optical and chemical properties showed a gradient MABr concentration structure in $MAPbBr_3$ films deposited using a modified two-step method. This from the gradient energy level can be beneficial for LED application by increasing the efficiency of charge transport and localization. Also, the interdiffusion process further intensified the gradient concentration structure and increased the luminescent efficiency to $CE_{max} = 0.861$ cd A^{-1} and $L_{max} = 604$ cd m^{-2}; these results show the great potential of the two-step deposition method to produce highly efficient PeLEDs by applying a general strategy to control the compositional engineering of MHPs.

See supplementary material for supporting figures associated with this article.

This work was supported by the National Research Foundation of Korea (NRF) grant funded by the Korea government (Ministry of Science, ICT and Future Planning) (No. NRF-2016R1A3B1908431); BK21PLUS SNU Materials Division for Educating Creative Global Leaders (No. 21A20131912052); Creative Materials Discovery Program through the National Research Foundation of Korea (NRF) funded by the Ministry of Science and ICT (No. 2018M3D1A1058536); the Nano Material Technology Development Program through the National Research Foundation of Korea (NRF) funded by the Ministry of Science, ICT and Future Planning (MSIP, Korea)

(No. NRF-2014M3A7B4051747); and NRF (National Research Foundation of Korea) grant funded by the Korean Government (No. NRF-2018H1A2A1062779-Global Ph.D. Fellowship Program).

[1] M. Liu, M. B. Johnston, and H. J. Snaith, Nature **501**, 395 (2013).
[2] W. S. Yang, J. H. Noh, N. J. Jeon, Y. C. Kim, S. Ryu, J. Seo, and S. I. Seok, Science **348**, 1234 (2015).
[3] W. S. Yang, B.-W. Park, E. H. Jung, and N. J. Jeon, Science **356**, 1376 (2017).
[4] S. D. Stranks, G. E. Eperon, G. Grancini, C. Menelaou, M. J. P. Alcocer, T. Leijtens, L. M. Herz, A. Petrozza, and H. J. Snaith, Science **342**, 341 (2013).
[5] A. A. Zhumekenov, M. I. Saidaminov, M. A. Haque, E. Alarousu, S. P. Sarmah, B. Murali, I. Dursun, X.-H. Miao, A. L. Abdelhady, T. Wu, O. F. Mohammed, and O. M. Bakr, ACS Energy Lett. **1**, 32 (2016).
[6] S. De Wolf, J. Holovsky, S.-J. Moon, P. Löper, B. Niesen, M. Ledinsky, F.-J. Haug, J.-H. Yum, and C. Ballif, J. Phys. Chem. Lett. **5**, 1035 (2014).
[7] Y. Wang, Y. Zhang, P. Zhang, and W. Zhang, Phys. Chem. Chem. Phys. **17**, 11516 (2015).
[8] F. Zhang, H. Zhong, C. Chen, X. Wu, X. Hu, H. Huang, J. Han, B. Zou, and Y. Dong, ACS Nano **9**, 4533 (2015).
[9] L. Protesescu, S. Yakunin, M. I. Bodnarchuk, F. Krieg, R. Caputo, C. H. Hendon, R. X. Yang, A. Walsh, and M. V. Kovalenko, Nano Lett. **15**, 3692 (2015).
[10] N. Wang, L. Cheng, R. Ge, S. Zhang, Y. Miao, W. Zou, C. Yi, Y. Sun, Y. Cao, R. Yang, Y. Wei, Q. Guo, Y. Ke, M. Yu, Y. Jin, Y. Liu, Q. Ding, D. Di, L. Yang, G. Xing, H. Tian, C. Jin, F. Gao, R. H. Friend, J. Wang, and W. Huang, Nat. Photonics **10**, 699 (2016).
[11] Y.-H. Kim, H. Cho, and T.-W. Lee, Proc. Natl. Acad. Sci. U. S. A. **113**, 11694 (2016).
[12] T. M. Brenner, D. A. Egger, L. Kronik, G. Hodes, and D. Cahen, Nat. Rev. Mater. **1**, 15007 (2016).
[13] Y.-H. Kim, H. Cho, J. H. Heo, T.-S. Kim, N. Myoung, C.-L. Lee, S. H. Im, and T.-W. Lee, Adv. Mater. **27**, 1248 (2015).
[14] Z.-K. Tan, R. S. Moghaddam, M. L. Lai, P. Docampo, R. Higler, F. Deschler, M. Price, A. Sadhanala, L. M. Pazos, D. Credgington, F. Hanusch, T. Bein, H. J. Snaith, and R. H. Friend, Nat. Nanotechnol. **9**, 687 (2014).
[15] H. Cho, S.-H. Jeong, M.-H. Park, Y.-H. Kim, C. Wolf, C.-L. Lee, J. H. Heo, A. Sadhanala, N. Myoung, S. Yoo, S. H. Im, R. H. Friend, and T.-W. Lee, Science **350**, 1222 (2015).
[16] M.-H. Park, S.-H. Jeong, H.-K. Seo, C. Wolf, Y.-H. Kim, H. Kim, J. Byun, J. S. Kim, H. Cho, and T.-W. Lee, Nano Energy **42**, 157 (2017).
[17] J.-W. Lee, Y. J. Choi, J.-M. Yang, S. Ham, S. K. Jeon, J. Y. Lee, Y.-H. Song, E. K. Ji, D.-H. Yoon, S. Seo, H. Shin, G. S. Han, H. S. Jung, D. Kim, and N.-G. Park, ACS Nano **11**, 3311 (2017).
[18] L. Zhao, Y.-W. Yeh, N. L. Tran, F. Wu, Z. Xiao, R. A. Kerner, Y. L. Lin, G. D. Scholes, N. Yao, and B. P. Rand, ACS Nano **11**, 3957 (2017).
[19] Z. Xiao, R. A. Kerner, L. Zhao, N. L. Tran, K. M. Lee, T. Koh, G. D. Scholes, and B. P. Rand, Nat. Photon. **11**, 108 (2017).
[20] H. Cho, J. S. Kim, C. Wolf, Y.-H. Kim, H. J. Yun, S.-H. Jeong, A. Sadhanala, V. Venugopalan, J. W. Choi, C.-L. Lee, R. H. Friend, and T.-W. Lee, ACS Nano **12**, 2883 (2018).
[21] H. P. Kim, J. Kim, B. S. Kim, H.-M. Kim, J. Kim, Abd. Rashid bin, M. Yusoff, J. Jang, and M. K. Nazeeruddin, Adv. Opt. Mater. **5**, 1600920 (2017).
[22] L. Zhang, X. Yang, Q. Jiang, P. Wang, Z. Yin, X. Zhang, H. Tan, Y. M. Yang, M. Wei, B. R. Sutherland, E. H. Sargent, and J. You, Nat. Commun. **8**, 15640 (2017).
[23] W. Zou, R. Li, S. Zhang, Y. Liu, N. Wang, Y. Cao, Y. Miao, M. Xu, Q. Guo, D. Di, L. Zhang, C. Yi, F. Gao, R. H. Friend, J. Wang, and W. Huang, Nat. Commun. **9**, 608 (2018).
[24] J. Chang, S. Zhang, N. Wang, Y. Sun, Y. Wei, R. Li, C. Yi, J. Wang, and W. Huang, J. Phys. Chem. Lett. **9**, 881 (2018).
[25] X. Yang, X. Zhang, J. Deng, Z. Chu, Q. Jiang, J. Meng, P. Wang, L. Zhang, Z. Yin, and J. You, Nat. Commun. **9**, 2 (2018).
[26] J. Byun, H. Cho, C. Wolf, M. Jang, A. Sadhanala, R. H. Friend, H. Yang, and T.-W. Lee, Adv. Mater. **28**, 7515 (2016).
[27] M. Yuan, L. N. Quan, R. Comin, G. Walters, R. Sabatini, O. Voznyy, S. Hoogland, Y. Zhao, E. M. Beauregard, P. Kanjanaboos, Z. Lu, D. H. Kim, and E. H. Sargent, Nat. Nanotechnol. **11**, 872 (2016).
[28] L. N. Quan, Y. Zhao, F. P. García de Arquer, R. Sabatini, G. Walters, O. Voznyy, R. Comin, Y. Li, J. Z. Fan, H. Tan, J. Pan, M. Yuan, O. M. Bakr, Z. Lu, D. H. Kim, and E. H. Sargent, Nano Lett. **17**, 3701 (2017).
[29] Y. F. Ng, S. A. Kulkarni, S. Parida, N. F. Jamaludin, N. Yantara, A. Bruno, C. Soci, S. Mhaisalkar, and N. Mathews, Chem. Commun. **53**, 12004 (2017).
[30] Y.-H. Kim, C. Wolf, Y.-T. Kim, H. Cho, W. Kwon, S. Do, A. Sadhanala, C. G. Park, S.-W. Rhee, S. H. Im, R. H. Friend, and T.-W. Lee, ACS Nano **11**, 6586 (2017).
[31] Y.-H. Kim, G.-H. Lee, Y.-T. Kim, C. Wolf, H. J. Yun, W. Kwon, C. G. Park, and T.-W. Lee, Nano Energy **38**, 51 (2017).
[32] X. Y. Chin, A. Perumal, A. Bruno, N. Yantara, S. Veldhuis, L. Martinez-Sarti, B. Chandran, V. S. Chirvony, S.-Z. A. Lo, J. So, C. Soci, M. Grätzel, H. J. Bolink, N. Mathews, and S. G. Mhaisalkar, Energy Environ. Sci. **11**, 1770 (2018).
[33] T. Chiba, K. Hoshi, Y.-J. Pu, Y. Takeda, Y. Hayashi, S. Ohisa, S. Kawata, and J. Kido, ACS Appl. Mater. Interfaces **9**, 18054 (2017).
[34] Z. Shi, S. Li, Y. Li, H. Ji, X. Li, D. Wu, T. Xu, Y. Chen, Y. Tian, Y. Zhang, C. Shan, and G. Du, ACS Nano **12**, 1462 (2018).
[35] S. Lee, J. H. Park, Y. S. Nam, B. R. Lee, B. Zhao, D. Di Nuzzo, E. D. Jung, H. Jeon, J. Kim, H. Y. Jeong, R. H. Friend, and M. H. Song, ACS Nano **12**, 3417 (2018).
[36] N. Yantara, S. Bhaumik, F. Yan, D. Sabba, H. A. Dewi, N. Mathews, P. P. Boix, H. V. Demir, and S. Mhaisalkar, J. Phys. Chem. Lett. **6**, 4360 (2015).
[37] Z. Wei, A. Perumal, R. Su, S. Sushant, J. Xing, Q. Zhang, S. T. Tan, H. V. Demir, and Q. Xiong, Nanoscale **8**, 18021 (2016).
[38] H. Cho, C. Wolf, J. S. Kim, H. J. Yun, J. S. Bae, H. Kim, J.-M. Heo, S. Ahn, and T.-W. Lee, Adv. Mater. **29**, 1700579 (2017).
[39] J. Li, S. G. R. Bade, X. Shan, and Z. Yu, Adv. Mater. **27**, 5196 (2015).
[40] Y. Ling, Y. Tian, X. Wang, J. C. Wang, J. M. Knox, F. Perez-Orive, Y. Du, L. Tan, K. Hanson, B. Ma, and H. Gao, Adv. Mater. **28**, 8983 (2016).
[41] P. Chen, Z. Xiong, X. Wu, M. Shao, X. Ma, Z. Xiong, and C. Gao, J. Phys. Chem. Lett. **8**, 1810 (2017).

[42] R. A. Kerner, L. Zhao, Z. Xiao, and B. P. Rand, J. Mater. Chem. A **4**, 8308 (2016).
[43] Z. Wang, Z. Luo, C. Zhao, Q. Guo, Y. Wang, F. Wang, X. Bian, A. Alsaedi, T. Hayat, and Z. Tan, J. Phys. Chem. C **121**, 28132 (2017).
[44] J. Burschka, N. Pellet, S.-J. Moon, R. Humphry-Baker, P. Gao, M. K. Nazeeruddin, and M. Grätzel, Nature **499**, 316 (2013).
[45] J.-H. Im, H.-S. Kim, and N.-G. Park, APL Mater. **2**, 081510 (2014).
[46] J.-H. Im, I.-H. Jang, N. Pellet, M. Grätzel, and N.-G. Park, Nat. Nanotechnol. **9**, 927 (2014).
[47] M. Becker and M. Wark, Org. Electron. **50**, 87 (2017).
[48] C. Motta, F. El-Mellouhi, S. Kais, N. Tabet, F. Alharbi, and S. Sanvito, Nat. Commun. **6**, 7026 (2015).
[49] N. K. Kumawat, N. Jain, A. Dey, K. L. Narasimhan, and D. Kabra, Adv. Funct. Mater. **27**, 1603219 (2017).
[50] Y. F. Ng, W. J. Neo, N. F. Jamaludin, N. Yantara, S. Mhaisalkar, and N. Mathews, Energy Technol. **5**, 1859 (2017).
[51] S.-Y. Kim, H. J. Jo, S.-J. Sung, and D.-H. Kim, APL Mater. **4**, 100901 (2016).
[52] F. Urbach, Phys. Rev. **92**, 1324 (1953).
[53] J. D. Dow and D. Redfield, Phys. Rev. B **5**, 594 (1972).
[54] I. Studenyak, M. Kranj, and M. Kurik, Int. J. Opt. Appl. **4**(3), 76 (2014).
[55] C. Wolf, J.-S. Kim, and T.-W. Lee, ACS Appl. Mater. Interfaces **9**, 10344 (2017).
[56] S. Singh, C. Li, F. Panzer, K. L. Narasimhan, A. Graeser, T. P. Gujar, A. Köhler, M. Thelakkat, S. Huettner, and D. Kabra, J. Phys. Chem. Lett. **7**, 3014 (2016).
[57] T. Meier, T. P. Gujar, A. Schönleber, S. Olthof, K. Meerholz, S. van Smaalen, F. Panzer, M. Thelakkat, and A. Köhler, J. Mater. Chem. C **6**, 7512 (2018).
[58] A. Al Mamun, T. T. Ava, H. J. Jeong, M. S. Jeong, and G. Namkoong, Phys. Chem. Chem. Phys. **19**, 9143 (2017).
[59] G. Namkoong, H. J. Jeong, A. Mamun, H. Byun, D. Demuth, and M. S. Jeong, Sol. Energy Mater. Sol. Cells **155**, 134 (2016).
[60] Q. Chen, H. Zhou, T. Bin Song, S. Luo, Z. Hong, H. S. Duan, L. Dou, Y. Liu, and Y. Yang, Nano Lett. **14**, 4158 (2014).
[61] T.-W. Ng, H. Thachoth Chandran, C.-Y. Chan, M.-F. Lo, and C.-S. Lee, ACS Appl. Mater. Interfaces **7**, 20280 (2015).
[62] B. Dänekamp, C. Müller, M. Sendner, P. P. Boix, M. Sessolo, R. Lovrincic, and H. J. Bolink, J. Phys. Chem. Lett. **9**, 2770 (2018).
[63] J. Yan, B. Zhang, Y. Chen, A. Zhang, and X. Ke, ACS Appl. Mater. Interfaces **8**, 12756 (2016).
[64] B. Zhang, J. Yan, J. Wang, and Y. Chen, Opt. Mater. **62**, 273 (2016).
[65] M. B. Johnston and L. M. Herz, Acc. Chem. Res. **49**, 146 (2016).
[66] Z. Chen, Z. Li, C. Zhang, X.-F. Jiang, D. Chen, Q. Xue, M. Liu, S. Su, H.-L. Yip, and Y. Cao, Adv. Mater. **30**, 1801370 (2018).
[67] D. W. de Quilettes, S. M. Vorpahl, S. D. Stranks, H. Nagaoka, G. E. Eperon, M. E. Ziffer, H. J. Snaith, and D. S. Ginger, Science **348**, 683 (2015).